ACS APPLIED MATERIALS & INTERFACES

Research Article

www.acsami.org

Influence of Number of Benzodioxan-Stilbazole-based Ancillary Ligands on Dye Packing, Photovoltage and Photocurrent in Dye-Sensitized Solar Cells

Hammad Cheema,[†] Ashraful Islam,[‡] Liyuan Han,[‡] and Ahmed El-Shafei*,[†]

[†]Polymer and Color Chemistry Program, North Carolina State University, Raleigh, North Carolina 27695, United States

[‡]Photovoltaic Materials Unit, National Institute for Materials Science, 1-2-1 Sengen, Tsukuba, Ibaraki 305-0047, Japan

Supporting Information

ABSTRACT: Two novel heteroleptic Ru(II) bipyridyl complexes, HD-2 and HD-2-mono, were molecularly engineered, synthesized and characterized for dye-sensitized solar cells (DSCs). The influences of mono versus bis electron-donor benzodioxan ancillary ligands on optical, dye packing, electrochemical and photovoltaic properties were examined and compared to the benchmark N719. HD-2 and HD-2-mono achieved solar-to-power conversion efficiencies (%η) of 9.64 and 9.50, respectively, compared to 9.32 for N719 under the same experimental device conditions. Optical results showed that HD-2 and HD-2-mono have much higher molar extinction coefficients, longer excited state lifetimes and narrower HOMO−LUMO gaps compared to N719. Although the molar extinction coefficient of HD-2-mono was 27% less than that of HD-2, it outperformed HD-2 in photovoltaic performance when anchored on TiO_2, owing to better dye packing and loading of the former. Charge recombination at the dye/TiO_2 interface by impedance spectroscopy analysis showed that the recombination resistance and the lifetime of injected electron in TiO_2 conduction band is directly proportional to the open-circuit voltage (V_{oc}) observed. Furthermore, compared to HD-2 and HD-2-mono, the greater V_{oc} of N719 can be attributed to the greater negative free energy for dye regeneration. Both HD-2 and HD-mono have almost the same negative free energy, which explains why they achieved almost the same V_{oc}. Decay dynamic analysis for solar devices fabricated from the named dyes, by time correlated single photon counting (TCSPC), elucidated that the lowest excited state decay lifetime for HD-2-mono, HD-2 and N719 are 3, 10 and 20 ps, respectively. The shorter the decay lifetime, the less kinetic redundancy, which leads to better photocurrent, and that explanation is consistent with the measured photocurrent and total solar-to-power conversion efficiency of the named dyes in the order of HD-2-mono > HD-2 > N719.

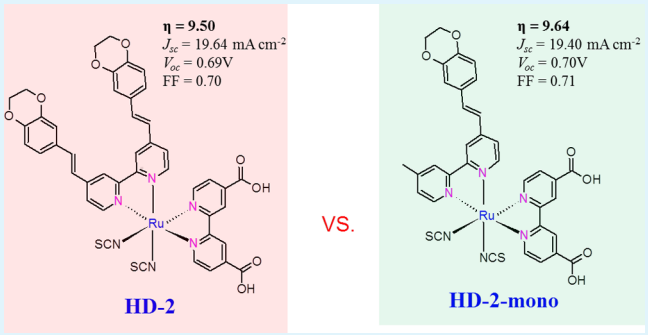

KEYWORDS: *dye-sensitized solar cells, mono versus bis-electron-donor ancillary ligands, solar-to-electric conversion, IPCE, Ru(II) bipyridyl complexes*

1. INTRODUCTION

Dye-sensitized solar cells (DSCs) are highly attractive due to features such as cost-effective, flexible, variety of colors and sustained efficiencies.[1−5] The seminal work in the field of DSC was reported in 1991 by O'Regan and Gräetzel.[5] Since then, their approach of adsorbing sensitizing dye on nanocrystalline TiO_2 has been widely studied, scrutinized and optimized. The crucial findings have been meticulously summarized in previous reviews.[6−10] All the important components of DSC system such as sensitizing dye, electrolyte, semiconductor (TiO_2), electrode substrate (TCO) and hole replenishing materials (Pt counter electrode) have been equally popular in research. Albeit it can be said without ambiguity that the component of DSCs which has enjoyed the prime status in DSC research are the sensitizers (dyes). Research groups around the world such as the Gräetzel and Nazeeruddin group (EPFL, Switzerland) for novel sensitizers and DSC materials, Liyuan Han group at NIMS, Tsukuba, Japan for novel DSC materials and cell optimization, Nanyang Technological University (NTU) Singapore group for NCS free sensitizers, Filippo De Angelis group for DSC computational modeling, Hagfeldt group Sweden and James Durrant England for physical aspects of DSC operations have contributed greatly to the fundamental understanding and innovation in DSC over the last 2 decades. Currently, the perovskite-sensitized solid state dye solar cells have reached record high efficiency of 15%,[11] whereas 12.3 (%η)[12] has been achieved by cosensitization of an organic sensitizer (Y123) and a Zn−porphyrin complex (YD2-o-C8).

In terms of the sensitizers, N719 (%η, 11.18) is a popular benchmark[13,14] from a research point of view. However, it lacks

Received: April 20, 2014
Accepted: June 9, 2014
Published: June 9, 2014

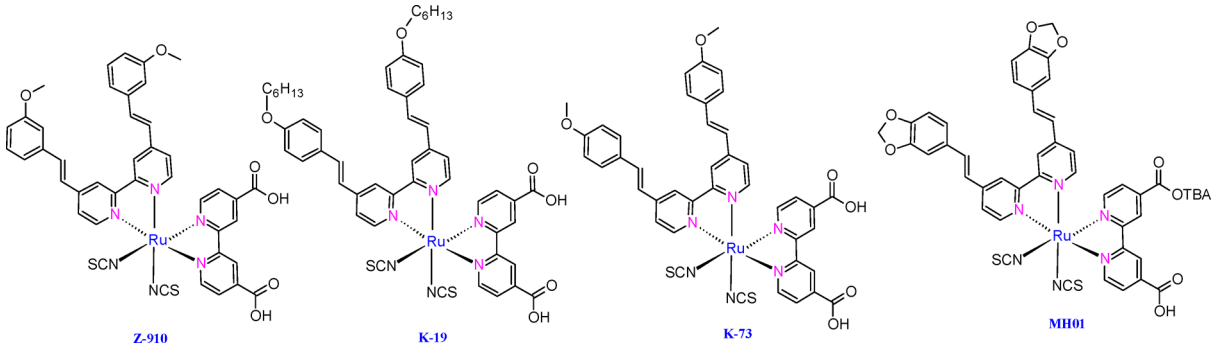

Figure 1. Molecular structures of complexes Z-910, K-19, K-73 and MH01-TBA.

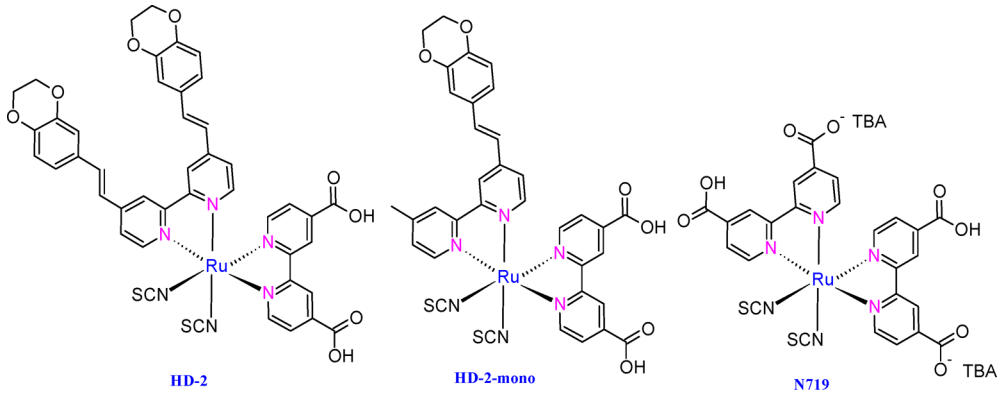

Figure 2. Molecular structures of complexes HD-2, HD-2-mono and N719.

absorption in the NIR region and exhibits low molar absorptivity and inefficient long-term stability. Development of panchromatic sensitizers is an active and ongoing area in DSC research.[15−19] The most successful strategies for designing of novel sensitizers include introduction of electron rich donors,[6,20−22] long alkyl chains,[23−25] thiocyanate free Ru(II) sensitizers[26−31] and sensitizers with spin-forbidden singlet-to-triplet transition for NIR response.[15,17,32] Oxygen containing electron donor ancillary ligands have been studied and are recognized as being potential candidates for DSCs as shown in Figure 1.[33−35] However, it was recently reported by El-Shafei et al.[22] that benzodioxole based cyclic ancillary ligand such as MH01-TBA, (%η) of 9.91 (Figure 1) are more promising than acyclic ancillary ligand analogues.

In this paper, as a continuation of this work, we report the synthesis and characterization of two novel sensitizers based on benzodioxan cyclic ancillary ligands as shown in Figure 2. We have investigated and compared the influence of mono (HD-2-mono) versus bis-ancillary ligands (HD-2) against the benchmark N719 in terms of light harvesting efficiency, optical, electrochemical, dye/TiO_2 interface characteristics, adsorption/packing difference at TiO_2 surface, decay dynamics and photovoltaic performance.

2. EXPERIMENTAL SECTION

2.1. Materials and Equipment. The solvents and chemicals were purchased from Sigma-Aldrich, Fisher Scientific or TCI-America and used as received. Sephadex LH-20 was purchased from Fisher Scientific. The mass spectrometry analysis was carried out on a high resolution mass spectrometer, the Thermo Fisher Scientific Exactive Plus MS, a benchtop full-scan OrbitrapTM mass spectrometer using heated electrospray ionization (HESI). Samples were dissolved in methanol and sonicated for 15 min. They were then diluted 1:1 with 20 mM ammonium acetate and analyzed via syringe injection into the mass spectrometer at a flow rate of 10 μL/min. The mass spectrometer was operated in negative ion mode. Fourier transform infrared spectroscopy (FT-IR) (ATR) spectra were recorded on a Nicolet Nexus 470 FT-IR spectrometer (Thermo Scientific, USA) and UV−visible spectra were measured by using Cary 300 spectrophotometer. Fluorescence and emission decay were recorded at room temperature on a Fluorolog-3 spectrofluorometer (HORIBA Jobin Yvon Inc.). ^{1}H NMR spectra were recorded using a Bruker 500 MHz or Varian 400 MHz spectrometer.

2.2. Synthesis of Ru(II) Sensitizers and Ancillary Ligands. For the synthesis of the proposed sensitizers, HD-2 and HD-2-mono, the corresponding ancillary ligands were synthesized according to the reported procedures[20,22] with modifications. The corresponding aromatic aldehydes and 4,4′-dimethyl-2,2′-bipyridyl were reacted in a pressure tube in the presence of chlorotrimethylsilane to produce the corresponding mono and bis-stilbazole in Knoevenagel condensation type reactions. The exact synthetic procedure can be found in the Supporting Information.

The proposed Ru(II) sensitizers were then synthesized in a typical one-pot three-steps synthetic scheme, as given in the Supporting Information. The yield of the crude products was in the range of 90−95%, which was purified through a Sephadex LH-20 column three times to obtain the highly pure product in 50−57% yield. The pure product was then characterized by ^{1}H NMR and high resolution mass spectrometry ($^-$ESI-MS).

2.3. Time Correlated Single Photon Counting (TCSPC) Measurements. Fluorescence spectra were recorded in a 1 cm path length quartz cell using 2×10^{-5} M solutions on a Fluorolog-311. The emitted light was detected in the steady state mode using a Hamamatsu R2658 detector. The emission was measured in the steady state mode by exciting at the metal-to-ligand charge transfer (MLCT) λ_{max} for each dye with exit and entrance slits set at 11 nm at an integration time of 0.1 s.

In the case of lifetime measurements, a time-correlated single photon counting method was employed on the solution of dyes in

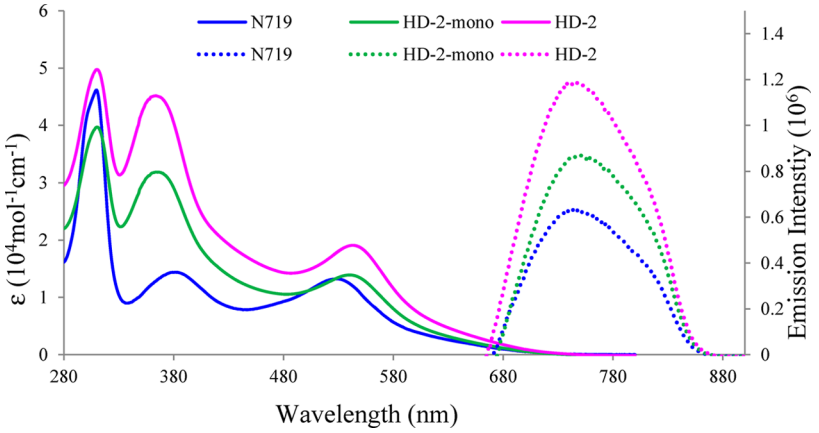

Figure 3. UV−vis absorption (solid line) and emission spectra (dashed line) of complexes HD-2 and HD-2-mono as compared to N719, measured in DMF (2×10^{-5} M).

DMF by exciting the samples using a pulse laser (460 nm, NanoLED) at a 1 MHz repetition rate with a band-pass of 15 nm. The time of arrival of the photon counting (TAC) range was adjusted to 200 ns in order to measure the emission decay lifetime (lowest excited state lifetime). The lifetime decay spectra were then fitted with DAS (data analysis software) from HORIBA Scientific. TCSPC studies on original cells were carried out using a similar method.

2.4. Ground State Oxidation Potential (GSOP) and Excited State Oxidation Potential (ESOP) Measurements. The GSOP and E_{0-0} energy values for HD-2 and HD-2-mono were measured using cyclic voltammetry (CV) and absorption/emission spectra point of overlap, respectively. In the CV experiment, the onset of oxidation was measured in DMF with 0.1 M [TBA][PF6] at a scan rate of 50 mV/s. Glassy carbon was used as the working electrode (WE), Pt wire as the counter electrode and Ag/Ag^+ in ACN was used as the reference electrode. Fc/Fc^+ was used as an internal reference, which was converted to NHE by addition of 0.63 V. Figures S11 and S12 (Supporting Information) show the CV graphs of HD-2 and HD-2-mono, respectively.

2.5. TiO_2 Electrode Preparation. A double-layer TiO_2 photoelectrode (10 + 5) μm in thickness with a 10 μm thick nanoporous layer and a 5 μm thick scattering layer (area: 0.25 cm^2) was prepared using a reported method.[13] Fluorine doped tin oxide-coated glass electrodes (Nippon Sheet Glass Co., Japan) with a sheet resistance of 8−10 ohm-2 and an optical transmission of greater than 80% in the visible range were screen printed using anatase TiO_2 colloids (particle size ~ 13 nm) obtained from commercial sources (Ti-Nanoxide D/SP, Solaronix). Nanocrystalline TiO_2 thin films were deposited onto the conducting glass by screen-printing, which was then sintered at 500 °C for 1 h. The film thickness was measured with a Surfcom 1400A surface profiler (Tokyo Seimitsu Co. Ltd.). The electrodes were impregnated with a 0.05 M titanium tetrachloride solution and sintered at 500 °C. The films were further treated with 0.1 M HCl(aq) before examination.[36] The dye solutions (2×10^{-4} M) were prepared in 1:1:1 mixture of acetonitrile, *tert*-butyl alcohol and dimethyl sulfoxide (DMSO). Deoxycholic acid was added to the dye solution as a coadsorbent at a concentration of 20 mM. The electrodes were immersed in the dye solutions and then kept at 25 °C for 20 h to adsorb the dye onto the TiO_2 surface.

2.6. Fabrication of Dye-Sensitized Solar Cell. Photovoltaic and incident photon-to-current efficiency (IPCE) measurements were made on sandwich cells, which were prepared using TiO_2 coated working electrodes and platinum coated counter electrodes, and were sealed using a 40 μm Syrlyn spacer through heating of the polymer frame. The redox electrolyte consisted of a solution of 0.6 M DMPII, 0.05 M I2, 0.1 M LiI and 0.5 M TBP in acetonitrile.

2.7. Photovoltaic Measurements. Photovoltaic measurements of sealed cells were made by illuminating the cell through the conducting glass from the anode side with a solar simulator (WXS-155S-10) at AM 1.5 illuminations (light intensity: 100 mW cm^{-2}).

2.8. IPCE Conversion. IPCE measurements were made on a CEP-2000 system (Bunkoh-Keiki Co. Ltd.). IPCE at each wavelength was calculated using eq 1, where ISC is the short-circuit photocurrent density (mA cm^{-2}) under monochromatic irradiation, q is the elementary charge, λ is the wavelength of incident radiation in nm and P_0 is the incident radiative flux in W/m^2.[37]

$$\mathrm{IPCE}(\lambda) = 1240\left(\frac{I_{SC}}{q\lambda P_0}\right) \quad (1)$$

The incident photon-to-current conversion efficiency was plotted as a function of wavelength.

2.9. Electrochemical Impedance Spectroscopy (EIS). The electrochemical impedance spectra were measured with an impedance analyzer in a potentiostat (Bio-Logic SP-150) under illumination using a solar simulator (SOL3A, Oriel) equipped with a 450 W xenon lamp (91160, Oriel). EIS spectra were recorded over a frequency range of 100 mHz to 200 kHz at 298 K. The applied bias voltage and AC amplitude were set at the open-circuit voltage (V_{oc}) of the DSCs, and the AC amplitude was set at 10 mV. The electrical impedance spectra were fitted using Z-Fit software (Bio-Logic).

3. RESULTS AND DISCUSSION

3.1. Photopysical Measurements. UV−vis absorption and emission spectra of HD-2, HD-2-mono and N719 were measured in DMF using a concentration of 2×10^{-5} M (Figure 3), and the results are summarized in Table 1.

Table 1. Absorption and Emission Properties for HD-2 and HD-2-mono as Compared to N719

sensitizer	absorption λ_{max} (nm)	ε (M^{-1} cm^{-1})	emission λ_{max} (nm)
HD-2	310, 364, 543 (d→π^*)	49750, 45150, 19100	740
HD-2-mono	310, 364, 539 (d→π^*)	39700, 31900, 13900	751
N719	310, 381, 529 (d→π^*)	46100, 14400, 12800	744

In Figure 3, the solid lines show the absorption spectra and dotted line show the emission for the same dye solutions, under the same conditions. Intense MLCT absorption peaks were found for HD-2 and HD-2-mono at 543 (19 100 M^{-1} cm^{-1}) and 539 (13 900 $M^{-1}cm^{-1}$), respectively, compared to N719 at 529 nm (12 800 M^{-1} cm^{-1}). It was observed that the HD-2-mono shows slightly blue shifted (5nm) spectra and a 27% decrease in the extinction coefficient compared to HD-2 for the low energy MLCT. This difference can be attributed to the

difference in the number of the electron donor ancillary ligands. Using the same concentration, the observed emission intensity was in the following order HD-2 > HD-2-mono > N719 due to the presence of stronger photon harvesting benzodioxan ancillary ligands as reported previously by El-Shafei el al. for other electron donating ancillary ligands.[20−22] To examine the effect of molecular modulation on the optical properties of mono (LH-2-mono) versus bis-ancillary ligands (LH-2), the absorption and emission spectra were performed. However, no significant difference in terms of λ_{max} for absorption or emission was observed, as shown in the Supporting Information, Figure S1.

When these ancillary ligands were complexed to Ru(II), however, more extended π-conjugation and more destabilization of the HOMO (t_{2g}) in HD-2 produced more red shift in the MLCT of HD-2 than HD-2-mono, and both were more red shifted than N719, as confirmed from E_{0-0}, GSOP and ESOP, as shown in the energy level diagram of Figure 4.

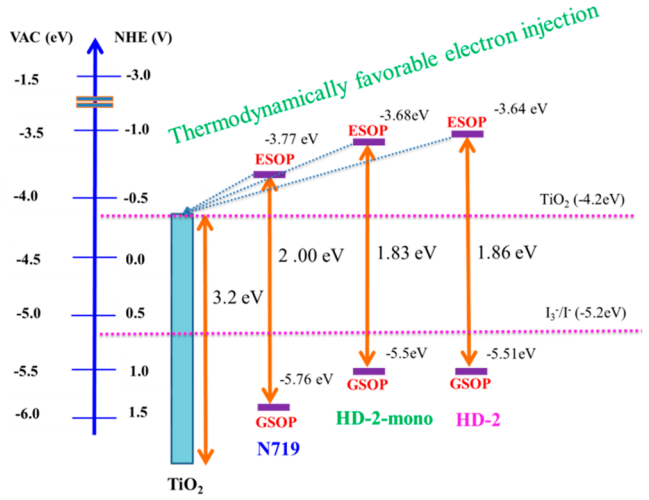

Figure 4. Energy level diagram and comparison between GSOP and ESOP of N719, HD-2-mono and HD-2.

3.2. Electrochemical Measurements. The ground state oxidation potential (GSOP) of HD-2 and HD-2-mono was measured by cyclic voltammetry (CV) in DMF. CV graphs (SI Figures S8−S9) were used to calculate the oxidation onset which is equivalent to the GSOP (ground state oxidation potential) or HOMO level of the dye. Additionally, E_{0-0} was calculated from the intersection point of experimental absorption and emission spectra and can be defined as the difference between the excited and ground state oxidation potentials. The values of E_{0-0} and GSOP were used to calculate the ESOP (excited state oxidation potential, the values in volts (V) against NHE were converted to electron volts (eV) according to eq 2.

$$\text{ESOP} = [(E_{0-0} + (\text{GSOP (V)} + 4.7)]\text{eV} \quad (2)$$

Following molecular modulation of ligands, there was no significant difference in E_{0-0}, GSOP and ESOP of the ancillary ligands LH-2 and LH-2-mono (Table 2). The GSOP values of −5.5 eV (0.8 V vs NHE) and −5.51 eV (0.81 V vs NHE) for HD-2 and HD-2-mono, respectively, provided enough thermodynamic driving force for electron replenishment by the I_3^-/I^- redox couple (−5.2 eV or −0.5 V vs NHE),[38] which leads to efficient dye regeneration. Additionally, ESOP of HD-2 and HD-2-mono were at −3.64 eV (−1.06 V vs NHE) and −3.68 eV (−1.02 V vs NHE), respectively, which lay above the conduction band edge of nanocrystalline TiO_2 (−4.2 eV).[39] Thus, thermodynamically favorable excited and ground states resulted in efficient electron injection into the CB edge of TiO_2 and dye regeneration sensitizers HD-2 and HD-2-mono, respectively. However, owing to more negative free energy of electron injection, HD-2 and HD-2-mono achieved greater photocurrent than that of N719. On the other hand, N719 had more negative free energy for dye regeneration, resulting in greater V_{oc}. A comparison of GSOP and ESOP for HD-2, HD-2-mono and N719 is given in Figure 4 and the results are summarized in Table 2.

Table 2. Excited State Oxidation Potential E^* and the Lowest Singlet−singlet Electronic Transitions (E_{0-0}) for HD-2, HD-2-mono and N719

	experimental (eV)		
sensitizer	$^aE_{0-0}$	^{b}GSOP(HOMO)	E^*
LH-2	3.21	−5.78	−2.57
LH-2-mono	3.25	−5.73	−2.53
HD-2	1.86	−5.5	−3.64
HD-2-mono	1.83	−5.51	−3.68
N719	1.99	−5.76	−3.77

$^aE_{0-0}$ = calculated from the intersection point of experimental absorption and emission spectra (DMF). ^{b}GSOP = ground state oxidation potential = E_{HOMO}; GSOP was measured in DMF with 0.1 M [TBA][PF6] and with a scan rate of 50 mV s^{-1}. It was calibrated with Fc/Fc^+ as internal reference and converted to NHE by addition of 0.63 V; excited-state oxidation potential, E^* was calculated from E^* = GSOP + $^*E_{0-0}$. Calculated GSOP, ESOP, and E_{0-0} of N719 was measured elsewhere.[40] E_{0-0}, GSOP and ESOP for ligands were calculated using a similar method as used for dyes.

3.3. Photovoltaic Device Characterizations. The photovoltaic performance of complexes HD-2 and HD-2-mono on nanocrystalline TiO_2 electrode was studied under standard AM 1.5 irradiation (100 mW cm^{-2}) using an electrolyte with a composition of 0.6 M dimethylpropylimidazolium iodide (DMPII), 0.05 M I_2, 0.1 M LiI in acetonitrile. Figure 5 shows the incident-photon-to-current efficiency conversion (IPCE) spectra for the cells fabricated with complexes HD-2,

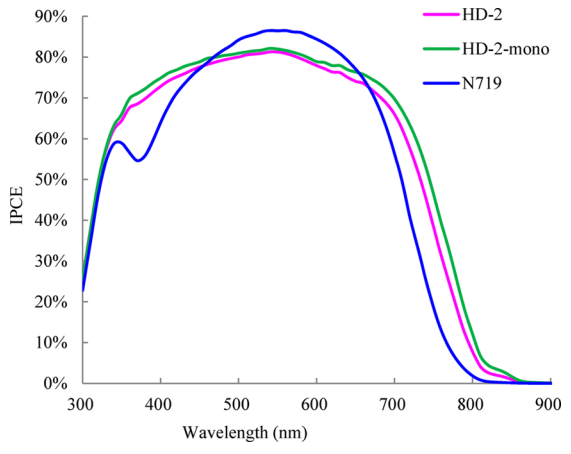

Figure 5. Photocurrent action spectra (IPCE) obtained with dyes HD-2-mono, HD-2 and N719 anchored on nanocrystalline TiO_2 film without additives *tert*-butylpyridine (TBP) and deoxycholic acid (DCA).

HD-2-mono and N719, where the IPCE values for each wavelength from 300 to 900 nm are plotted as a function of wavelength.

Owing to a stronger photon harvesting capability of benzodioxan-based ancillary ligands, sensitization over a broad wavelength range including the entire visible spectrum and near IR region was achieved. HD-2 and HD-2-mono outperformed N719 in IPCE in the wavelength ranges of 300−400 and 750−850 nm. The impressive quantum efficiency of up to 80% was achieved with both HD-2-mono and HD-2 in the wavelength range of 500−600 nm. The superior quantum efficiency of HD-2 and HD-2-mono compared to N719 translated into higher photocurrent density and higher (%η), as shown in Figure 6.

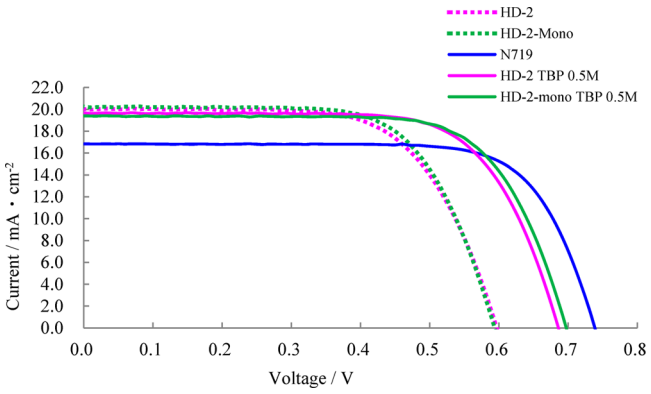

Figure 6. Photocurrent−voltage characteristics of DSCs sensitized with the complexes HD-2, HD-2-mono and N719 electrolyte, 0.6 M DMPII, 0.1 M LiI, 0.05 I_2 in acetonitrile (AN). Without additives (dotted line) and with additives (solid lines) TBP and DCA 20 mM.

The photovoltaic parameters including the short-circuit photocurrent density (J_{sc}), open-circuit voltage (V_{oc}), fill factors (FF) and overall cell efficiencies (%η) are summarized in Table 3.

Table 3. Photovoltaic Characteristics of HD-2, HD-2-mono and N719[a]

sensitizer	TBP (M)	J_{sc}(mA cm^{-2})	V_{oc} (V)	FF	η (%)
HD-2-mono	0.0	20.25	0.59	0.67	8.00
	0.5	19.40	0.70	0.71	9.64
HD-2	0.0	20.02	0.60	0.66	7.93
	0.5	19.67	0.69	0.70	9.50
N719	0.5	16.85	0.75	0.74	9.35

[a]Conditions: sealed cells; coadsorbate, DCA 20 mM; photoelectrode, TiO_2 (15 μm thickness and 0.25 cm^2); electrolyte, 0.6 M DMPII, 0.1 M LiI, 0.05 I_2 in AN; irradiated light, AM 1. Five solar light (100 mW cm^{-2}). J_{sc}, short-circuit photocurrent density; V_{oc}, open-circuit photovoltage; FF, fill factor; η, total power conversion efficiency.

HD-2-mono and HD-2 resulted in photocurrent densities (J_{sc}) of 20.25 and 20.02 mA cm^{-2}, respectively, without TBP, corresponding to an overall efficiency (%η) of 8.00 and 7.93, respectively. The J_{sc} of 20.25 mA cm^{-2} for HD-2-mono, which is 20% higher than the J_{sc} of N719, can be attributed to the greater photon harvesting and more energetically favorable electron injection into TiO_2 as supported by a higher molar extinction coefficient results and energy values of GSOP and ESOP (Figure 5). Addition of 0.5 M TBP resulted in a J_{sc} of 19.40 mA cm^{-2} and V_{oc} of 0.70 V, translating into a total conversion efficiency (%η) of 9.64 for HD-2-mono, surpassing the benchmark N719 (%η) of 9.32% and HD-2 of 9.50%.

To determine the best working conditions for HD-2 and HD-2-mono in the presence of TBP and DCA, solar cells were tested with different concentrations of TBP and DCA. TBP is well-known for its effect on suppressing the recombinations of injected electrons with I_3^- in electrolyte. TBP causes a negative increase in the conduction band edge of TiO_2, due to its basicity,[41−43] thus leading to higher V_{oc}. An increase in electron lifetime,[6] suppression of surface defects[44] and decrease in loss of $^-$NCS[45] is also reported to be caused by the presence of TBP.

Similarly, DCA as a coadsorber, can be added to the dye solution to achieve TiO_2 surface passivation, which suppresses the recombination reactions (dark current). Coadsorbers are also thought to assist in favorable packing of the dye on TiO_2 surface.[46] It was observed that 0.5 M TBP in the electrolyte solution works best with 20 mM of coadsorbate in the dye solution. The comparison results of IPCE and $I-V$ curves are shown in the Supporting Information, Figures S11 and S12.

Under optimized cell working conditions, HD-2 and HD-2-mono did not show substantial differences in V_{oc}, which contradicted the previous reports[47,48] of lower V_{oc} for bis-based dyes due to decreased loading. In comparison to sensitizers reported in previous studies,[47,48] a benzodioxan-based ligand is much smaller in size, hence, HD-2 and HD-2-mono are expected to exhibit no-to-little influence on dye loading. Figure 7 shows the HD-2 and HD-2-mono photo anodes after

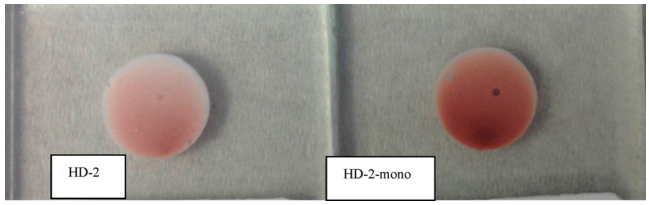

Figure 7. TiO_2 Electrodes after desorption of HD-2 and HD-2-mono with 0.1 M NaOH(aq) and DMF (1:1).

desorption of dye by dipping in 0.1 M NaOH(aq) and DMF (1:1) for 72 h. The visual difference in two electrodes can be correlated to the desorption and packing difference of the two dyes. Thus, we postulate that HD-2-mono is more resistant to desorption, owing to its small molecular size, which resulted in better packing on the TiO_2 surface. To completely desorb the dye from TiO_2, a mixture of 0.1 M TBAOH dissolved in MeOH and 0.1 M NaOH (1:1) was used. Complete desorption was achieved within 24 h for both HD-2 and HD-2-mono. Under similar conditions, the amount of dye desorbed was 1.5 × 10^{-5} mol cm^{-2} for HD-2 and 1.55 × 10^{-5} mol cm^{-2} for HD-2-mono. The amount of dye loading was up to 5% higher for HD-2-mono compared to HD-2, which confirms better packing of HD-2 mono, and that can be attributed to the small molecular size compared to HD-2. UV−vis for the desorbed dye solutions is given in Figure S11 (Supporting Information).

3.4. Electrochemical Impedance Spectroscopy Characterization. Interfacial charge transfer process at TiO_2/electrolyte and pt/electrolyte interfaces can be characterized by electrochemical impedance spectroscopy (EIS).[22,49] EIS is a key technique to study the passive electrical systems. Impedance measures the dielectric properties of a material and interface as the function of frequency. The EIS Nyquist and Bode plots for

the DSCs based on HD-2, HD-2-mono and N719 are shown in Figures 8 and 9, respectively. In EIS Nyquist plots, the

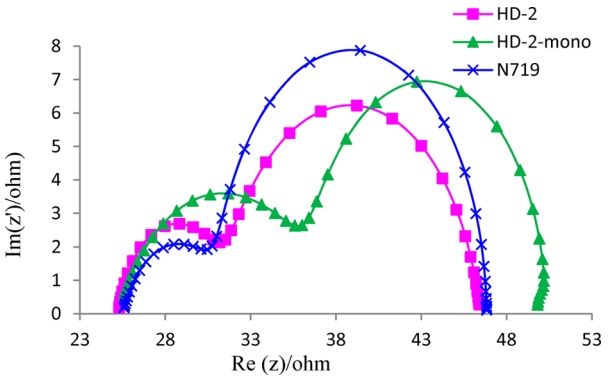

Figure 8. EIS Nyquist plots for DSCs sensitized with HD-2 and NCSU-10.

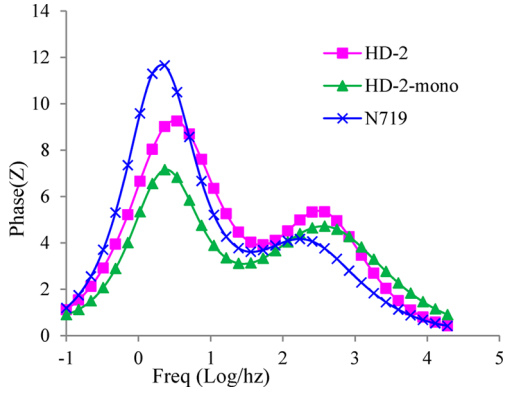

Figure 9. EIS Bode plots for DSCs sensitized with HD-2 and HD-2-mono and N719.

intermediate frequency range indicates the electron recombination resistance, which was in the following order N719 > HD-2-mono > HD-2, consistent with the V_{oc} of the devices, N719 > HD-2-mono > HD-2.

In Figure 9, the frequency response regime in the range of 1−100 Hz is an indicator of the electron recombination between electrolyte and TiO_2 and is related to the electron lifetime in the CB of TiO_2. The electron lifetime depends on the density of charge traps, which is ultimately related to V_{oc}. The middle-frequency peak of the DSCs based on HD-2-mono and N719 were observed to be slightly shifted to low frequency compared to HD-2 (Figure 9), indicating a shorter recombination lifetime for the latter case, thus resulting in a slightly lower V_{oc} for HD-2.

3.5. TCSPC Measurements. The TCSPC (time correlated single photon counting) method was employed to study the emission decay behavior of the dyes in solution and in the cell form. Figure S14 (inset) (Supporting Information) shows the lowest excited state decay behavior of the dyes in DMF. All of the decay curves were fitted with 2-exponential showing the multiexponental decay behavior having fast (shorter lifetime) and slow (longer lifetime) components. However, the relative amplitude of the fast component (B1) for N719 was too small as compared to HD-2 and HD-2-mono and can be ignored. The reported value of lowest excited state lifetime for N719 in air saturated ethanol solution is 40 ns[2], which in our case, was 38 ns in DMF, with HD-2 and HD-2-mono exhibiting the lowest excited state lifetimes of 58 ns and 49 ns, respectively, as given in Table S1 (Supporting Information).

TCSPC is the method of choice for studying the component of excited electron decay in DSCs,[50,51] which falls in the picosecond time range. According to TCSPC results on the complete DSC, the decay rate was in the following order: HD-2-mono > HD-2 > N719, as summarized in Table S1 (Supporting Information), and shown in Figure S14 (Supporting Information). The lowest excited state lifetime in DSC for HD-2-mono was found to be 3 ps as compared to 10 ps for HD-2 and 20 ps for N719. The observed decay rate is in excellent agreement with the overall cell efficiency of solar devices. Thus, we can postulate that the shorter the decay rate of the lowest excited state lifetime in DSC, the better the solar-to-power conversion efficiency, owing to more efficient injection and shorter recombination time of the excited electrons.

Hence, it can be postulated that the faster the decay rate of the lowest excited state lifetime, the better the J_{sc}, owing to more efficient electron injection caused by decrease in kinetic redundancy of the excited electrons. Durrant et al.[50,51] found that the optimum DSC performance can be ensured by having the charge separation kinetics just fast enough to compete with the excited state decay rate. Because electron injection from excited dye to TiO_2 conduction band happens in a femtosecond-picoseond[6,14,52] time range, the shorter picosecond lifetime component of the excited dye molecule is expected to result in a decrease in kinetic redundancy.

4. CONCLUSIONS

In summary, this study reports novel benzodioxan-based ligands for DSC, which are proven to be highly efficient sensitizers for DSCs. Solar cells based on Ru(II) sensitizers containing benzodioxan ligands showed solar-to-power conversion efficiency (%η) of up to 9.64 for HD-2-mono and 9.50 for HD-2, compared to 9.32 for the benchmark, N719. the smaller size sensitizer, HD-2-mono, showed up to 5% higher loading onto TiO_2 compared to HD-2. The reported sensitizers showed impressively higher photocurrent densities, which can be attributed to greater negative free energy of the excited state compared to that of N719. According to impedance spectroscopy results, recombination resistance and recombination lifetime for injected electrons into TiO_2 conduction band were observed to be in the same order as the V_{oc} of solar devices. The TCSPC decay rate performed on the devices was found to be in excellent agreement with (%η), HD-2-mono > HD-2 > N719, where shorter lifetime decay decreases the kinetic redundancy in the device. Thus, we clearly demonstrated by molecular modulation of ancillary ligands (mono versus bis), material consumption can be reduced without sacrificing overall efficiency by using mono ancillary ligands that are strong electron donors. We believe that this strategy could lead to a paradigm shift in the future design of novel Ru(II) sensitizers for DSCs by making smaller molecular sized sensitizers that are more efficient in solar-to-electric conversion.

■ ASSOCIATED CONTENT

Supporting Information

Synthesis details, FT-IR, high-resolution ESI-MS, ^{1}H NMR and cyclic voltammetry graphs. This material is available free of charge via the Internet at http://pubs.acs.org.

AUTHOR INFORMATION

Corresponding Author

*Ahmed El-Shafei. E-mail: Ahmed_El-Shafei@ncsu.edu.

Notes

The authors declare no competing financial interest.

REFERENCES

(1) Nazeeruddin, M. K.; Zakeeruddin, S. M.; Humphry-Baker, R.; Jirousek, M.; Liska, P.; Vlachopoulos, N.; Shklover, V.; Fischer, C.; Gräetzel, M. Acid-Base Equilibria of (2,2-Bipyridyl-4,4-dicarboxylic acid)ruthenium(II) Complexes and the Effect of Protonation on Charge-Transfer Sensitization of Nanocrystalline Titania. *Inorg. Chem.* **1999**, *38*, 6298−6305.

(2) Péchy, P.; Renouard, T.; Zakeeruddin, S. M.; Humphry-Baker, R.; Comte, P.; Liska, P.; Cevey, L.; Costa, E.; Shklover, V.; Spiccia, L.; Deacon, G. B.; Bignozzi, C. A.; Grätzel, M. Engineering of Efficient Panchromatic Sensitizers for Nanocrystalline TiO_2-Based Solar Cells. *J. Am. Chem. Soc.* **2001**, *123*, 1613−1624.

(3) Grätzel, C.; Zakeeruddin, S. M. Recent Trends in Mesoscopic Solar Cells Based On Molecular and Nanopigment Light Harvesters. *Mater. Today* **2013**, *16*, 11−18.

(4) Zhang, S.; Yang, X.; Numata, Y.; Han, L. Highly Efficient Dye-Sensitized Solar Cells: Progress and Future Challenges. *Energy Environ. Sci.* **2013**, *6*, 1443−1464.

(5) O'Regan, B.; Gräetzel, M. A Low-Cost, High-Efficiency Solar Cell Based On Dye-Sensitized Colloidal TiO_2 Films. *Nature* **1991**, *353*, 737−740.

(6) Hagfeldt, A.; Boschloo, G.; Sun, L.; Kloo, L.; Pettersson, H. Dye-Sensitized Solar Cells. *Chem. Rev.* **2010**, *110*, 6595−6663.

(7) Mishra, A.; Fischer, M. .; Bäuerle, P. Metal-Free Organic Dyes for Dye-Sensitized Solar Cells: From Structure: Property Relationships to Design Rules. *Angew. Chem., Int. Ed.* **2009**, *48*, 2474−2499.

(8) Ahmad, S.; Guillen, E.; Kavan, L.; Gratzel, M.; Nazeeruddin, M. K. Metal Free Sensitizer and Catalyst for Dye Sensitized Solar Cells. *Energy Environ. Sci.* **2013**, *6*, 3439−3466.

(9) Yen, Y.; Chou, H.; Chen, Y.; Hsu, C.; Lin, J. T. Recent Developments in Molecule-Based Organic Materials for Dye-Sensitized Solar Cells. *J. Mater. Chem.* **2012**, *22*, 8734−8747.

(10) Zhang, S.; Yang, X.; Numata, Y.; Han, L. Highly Efficient Dye-Sensitized Solar Cells: Progress And Future Challenges. *Energy Environ. Sci.* **2013**, *6*, 1443−1464.

(11) Burschka, J.; Pellet, N.; Moon, S.; Humphry-Baker, R.; Gao, P.; Nazeeruddin, M. K.; Gratzel, M. Sequential Deposition As A Route To High-Performance Perovskite-Sensitized Solar Cells. *Nature* **2013**, *499*, 316−319.

(12) Yella, A.; Lee, H.; Tsao, H. N.; Yi, C.; Chandiran, A. K.; Nazeeruddin, M. K.; Diau, E. W.; Yeh, C.; Zakeeruddin, S. M.; Grätzel, M. Porphyrin-Sensitized Solar Cells with Cobalt (II/III)-Based Redox Electrolyte Exceed 12% Efficiency. *Science* **2011**, *334*, 629−634.

(13) Nazeeruddin, M. K.; Splivallo, R.; Liska, P.; Comte, P.; Gratzel, M. A Swift Dye Uptake Procedure For Dye Sensitized Solar Cells. *Chem. Commun.* **2003**, *0*, 1456−1457.

(14) Grätzel, M. Conversion Of Sunlight To Electric Power By Nanocrystalline Dye-Sensitized Solar Cells. *J. Photochem. Photobiol., A* **2004**, *164*, 3−14.

(15) Kinoshita, T.; Dy, J. T.; Uchida, S.; Kubo, T.; Segawa, H. Wideband Dye-Sensitized Solar Cells Employing a Phosphine-Coordinated Ruthenium Sensitizer. *Nat. Photonics* **2013**, *7*, 535−539.

(16) Chou, C.; Hu, F.; Yeh, H.; Wu, H.; Chi, Y.; Clifford, J. N.; Palomares, E.; Liu, S.; Chou, P.; Lee, G. Highly Efficient Dye-Sensitized Solar Cells Based on Panchromatic Ruthenium Sensitizers with Quinolinylbipyridine Anchors. *Angew. Chem., Int. Ed.* **2014**, *53*, 178−183.

(17) Fantacci, S.; Ronca, E.; De Angelis, F. Impact of Spin−Orbit Coupling on Photocurrent Generation in Ruthenium Dye-Sensitized Solar Cells. *J. Phys. Chem. Lett.* **2014**, *5*, 375−380.

(18) Srimath Kandada, A. R.; Fantacci, S.; Guarnera, S.; Polli, D.; Lanzani, G.; De Angelis, F.; Petrozza, A. Role of Hot Singlet Excited States in Charge Generation at the Black Dye/TiO_2 Interface. *ACS Appl. Mater. Interfaces* **2013**, *5*, 4334−4339.

(19) Yang, J.; Ganesan, P.; Teuscher, J.; Moehl, T.; Kim, Y. J.; Yi, C.; Comte, P.; Pei, K.; Holcombe, T. W.; Nazeeruddin, M. K.; Hua, J.; Zakeeruddin, S. M.; Tian, H.; Gräetzel, M. Influence of the Donor Size in D-π-A Organic Dyes for Dye-Sensitized Solar Cells. *J. Am. Chem. Soc.* **2014**, *136*, 5722−5730.

(20) El-Shafei, A.; Hussain, M.; Atiq, A.; Islam, A.; Han, L. A Novel Carbazole-Based Dye Outperformed the Benchmark Dye N719 For High Efficiency Dye-Sensitized Solar Cells (DSSCs). *J. Mater. Chem.* **2012**, *22*, 24048−24056.

(21) El-Shafei, A.; Hussain, M.; Islam, A.; Han, L. Structure-Property Relationship of Extended Small π-Conjugation of Ancillary Ligands With And Without Electron Donor Of Heteroleptic Ru(II) Bipyridyl Complexes For High Efficiency Dye-Sensitized Solar Cells. *Phys. Chem. Chem. Phys.* **2013**, *15*, 8401−8408.

(22) El-Shafei, A.; Hussain, M.; Islam, A.; Han, L. Influence of Cyclic Versus Acyclic Oxygen-Containing Electron Donor Ancillary Ligands on the Photocurrent, Photovoltage and Photostability for High Efficiency Dye-Sensitized Solar Cells. *J. Mater. Chem. A* **2013**, *1*, 13679−13686.

(23) Schmidt-Mende, L.; Kroeze, J. E.; Durrant, J. R.; Nazeeruddin, M. K.; Gräetzel, M. Effect of Hydrocarbon Chain Length of Amphiphilic Ruthenium Dyes on Solid-State Dye-Sensitized Photovoltaics. *Nano Lett.* **2005**, *5*, 1315−1320.

(24) Klein, C.; Nazeeruddin, M. K.; Liska, P.; Di Censo, D.; Hirata, N.; Palomares, E.; Durrant, J. R.; Gräetzel, M. Engineering of a Novel Ruthenium Sensitizer and Its Application in Dye-Sensitized Solar Cells for Conversion of Sunlight into Electricity. *Inorg. Chem.* **2005**, *44*, 178−180.

(25) Wang, P.; Zakeeruddin, S. M.; Moser, J. E.; Nazeeruddin, M. K.; Sekiguchi, T.; Gratzel, M. A Stable Quasi-Solid-State Dye-Sensitized Solar Cell with an Amphiphilic Ruthenium Sensitizer and Polymer Gel Electrolyte. *Nat. Mater.* **2003**, *2*, 402−407.

(26) Chen, B.; Chen, K.; Hong, Y.; Liu, W.; Li, T.; Lai, C.; Chou, P.; Chi, Y.; Lee, G. Neutral, Panchromatic Ru(II) Terpyridine Sensitizers Bearing Pyridine Pyrazolate Chelates With Superior DSSC Performance. *Chem. Commun.* **2009**, *0*, 5844−5846.

(27) Singh, S. P.; Gupta, K. S. V.; Sharma, G. D.; Islam, A.; Han, L. Efficient Thiocyanate-Free Sensitizer: A Viable Alternative To N719 Dye For Dye-Sensitized Solar Cells. *Dalton Trans.* **2012**, *41*, 7604−7608.

(28) Wu, K.; Hsu, H.; Chen, K.; Chi, Y.; Chung, M.; Liu, W.; Chou, P. Development of Thiocyanate-Free, Charge-Neutral Ru(II) Sensitizers For Dye-Sensitized Solar Cells. *Chem. Commun.* **2010**, *46*, 5124−5126.

(29) Chou, C.; Wu, K.; Chi, Y.; Hu, W.; Yu, S. J.; Lee, G.; Lin, C.; Chou, P. Ruthenium(II) Sensitizers with Heteroleptic Tridentate Chelates for Dye-Sensitized Solar Cells. *Angew. Chem., Int. Ed.* **2011**, *50*, 2054−2058.

(30) Yang, S.; Wu, K.; Chi, Y.; Cheng, Y.; Chou, P. Tris(thiocyanate) Ruthenium(II) Sensitizers with Functionalized Dicarboxyterpyridine for Dye-Sensitized Solar Cells. *Angew. Chem., Int. Ed.* **2011**, *50*, 8270−8274.

(31) Wu, K.; Ku, W.; Clifford, J. N.; Palomares, E.; Ho, S.; Chi, Y.; Liu, S.; Chou, P.; Nazeeruddin, M. K.; Gratzel, M. Harnessing The Open-Circuit Voltage Via a New Series Of Ru(II) Sensitizers Bearing (Iso-)Quinolinyl Pyrazolate Ancillaries. *Energy Environ. Sci.* **2013**, *6*, 859−870.

(32) Kinoshita, T.; Fujisawa, J.; Nakazaki, J.; Uchida, S.; Kubo, T.; Segawa, H. Enhancement of Near-IR Photoelectric Conversion in Dye-Sensitized Solar Cells Using an Osmium Sensitizer with Strong Spin-Forbidden Transition. *J. Phys. Chem. Lett.* **2012**, *3*, 394−398.

(33) Wang, P.; Zakeeruddin, S.; Moser, J. .; Humphry-Baker, R.; Comte, P.; Aranyos, V.; Hagfeldt, A.; Nazeeruddin, M. .; Grätzel, M. Stable New Sensitizer with Improved Light Harvesting for Nanocrystalline Dye-Sensitized Solar Cells. *Adv. Mater.* **2004**, *16*, 1806−1811.

(34) Wang, P.; Klein, C.; Humphry-Baker, R.; Zakeeruddin, S. M.; Gräetzel, M. A High Molar Extinction Coefficient Sensitizer for Stable Dye-Sensitized Solar Cells. *J. Am. Chem. Soc.* **2005**, *127*, 808−809.
(35) Kuang, D.; Ito, S.; Wenger, B.; Klein, C.; Moser, J.; Humphry-Baker, R.; Zakeeruddin, S. M.; Gräetzel, M. High Molar Extinction Coefficient Heteroleptic Ruthenium Complexes for Thin Film Dye-Sensitized Solar Cells. *J. Am. Chem. Soc.* **2006**, *128*, 4146−4154.
(36) Wang, Z.; Yamaguchi, T.; Sugihara, H.; Arakawa, H. Significant Efficiency Improvement of the Black Dye-Sensitized Solar Cell through Protonation of TiO_2 Films. *Langmuir* **2005**, *21*, 4272−4276.
(37) Islam, A.; Chowdhury, F. A.; Chiba, Y.; Komiya, R.; Fuke, N.; Ikeda, N.; Nozaki, K.; Han, L. Synthesis and Characterization of New Efficient Tricarboxyterpyridyl ($\hat{I}^2$-diketonato) Ruthenium(II) Sensitizers and Their Applications in Dye-Sensitized Solar Cells. *Chem. Mater.* **2006**, *18*, 5178−5185.
(38) Qu, P.; Meyer, G. J. Proton-Controlled Electron Injection from Molecular Excited States to the Empty States in Nanocrystalline TiO_2. *Langmuir* **2001**, *17*, 6720−6728.
(39) Oskam, G.; Bergeron, B. V.; Meyer, G. J.; Searson, P. C. Pseudohalogens for Dye-Sensitized TiO_2 Photoelectrochemical Cells. *J. Phys. Chem. B* **2001**, *105*, 6867−6873.
(40) De Angelis, F.; Fantacci, S.; Selloni, A.; Nazeeruddin, M. K.; Gräetzel, M. First-Principles Modeling of the Adsorption Geometry and Electronic Structure of Ru(II) Dyes on Extended TiO_2 Substrates for Dye-Sensitized Solar Cell Applications. *J. Phys. Chem. C* **2010**, *114*, 6054−6061.
(41) Schlichthqrl, G.; Huang, S. Y.; Sprague, J.; Frank, A. J. Band Edge Movement and Recombination Kinetics in Dye-Sensitized Nanocrystalline TiO_2 Solar Cells: A Study by Intensity Modulated Photovoltage Spectroscopy. *J. Phys. Chem. B* **1997**, *101*, 8141−8155.
(42) Hara, K.; Dan-oh, Y.; Kasada, C.; Ohga, Y.; Shinpo, A.; Suga, S.; Sayama, K.; Arakawa, H. Effect of Additives on the Photovoltaic Performance of Coumarin-Dye-Sensitized Nanocrystalline TiO_2 Solar Cells. *Langmuir* **2004**, *20*, 4205−4210.
(43) Haque, S. A.; Tachibana, Y.; Willis, R. L.; Moser, J. E.; Gräetzel, M.; Klug, D. R.; Durrant, J. R. Parameters Influencing Charge Recombination Kinetics in Dye-Sensitized Nanocrystalline Titanium Dioxide Films. *J. Phys. Chem. B* **2000**, *104*, 538−547.
(44) Yin, X.; Zhao, H.; Chen, L.; Tan, W.; Zhang, J.; Weng, Y.; Shuai, Z.; Xiao, X.; Zhou, X.; Li, X.; Lin, Y. The Effects of Pyridine Derivative Additives On Interface Processes at Nanocrystalline TiO_2 Thin Film In Dye-Sensitized Solar Cells. *Surf. Interface Anal.* **2007**, *39*, 809−816.
(45) Greijer, H.; Lindgren, J.; Hagfeldt, A. Resonance Raman Scattering of a Dye-Sensitized Solar Cell: Mechanism of Thiocyanato Ligand Exchange. *J. Phys. Chem. B* **2001**, *105*, 6314−6320.
(46) Neale, N. R.; Kopidakis, N.; van, d. L.; Gräetzel, M.; Frank, A. J. Effect of a Coadsorbent on the Performance of Dye-Sensitized TiO_2 Solar Cells: Shielding versus Band-Edge Movement. *J. Phys. Chem. B* **2005**, *109*, 23183−23189.
(47) Choi, H.; Baik, C.; Kim, S.; Kang, M.; Xu, X.; Kang, H. S.; Kang, S. O.; Ko, J.; Nazeeruddin, M. K.; Gratzel, M. Molecular Engineering of Hybrid Sensitizers Incorporating an Organic Antenna into Ruthenium Complex and Their Application In Solar Cells. *New J. Chem.* **2008**, *32*, 2233−2237.
(48) Jung, I.; Choi, H.; Lee, J. K.; Song, K. H.; Kang, S. O.; Ko, J. New Ruthenium Sensitizers Containing Styryl and Antenna Fragments. *Inorg. Chim. Acta* **2007**, *360*, 3518−3524.
(49) Koide, N.; Islam, A.; Chiba, Y.; Han, L. Improvement of Efficiency of Dye-Sensitized Solar Cells Based on Analysis of Equivalent Circuit. *J. Photochem. Photobiol., A* **2006**, *182*, 296−305.
(50) Koops, S. E.; Durrant, J. R. Transient Emission Studies of Electron Injection in Dye Sensitized Solar Cells. *Inorg. Chim. Acta* **2008**, *361*, 663−670.
(51) Haque, S. A.; Palomares, E.; Cho, B. M.; Green, A. N. M.; Hirata, N.; Klug, D. R.; Durrant, J. R. Charge Separation versus Recombination in Dye-Sensitized Nanocrystalline Solar Cells: the Minimization of Kinetic Redundancy. *J. Am. Chem. Soc.* **2005**, *127*, 3456−3462.
(52) Hannappel, T.; Burfeindt, B.; Storck, W.; Willig, F. Measurement of Ultrafast Photoinduced Electron Transfer from Chemically Anchored Ru-Dye Molecules into Empty Electronic States in a Colloidal Anatase TiO_2 Film. *J. Phys. Chem. B* **1997**, *101*, 6799−6802.